

**₁ Drift and mixing under the ocean surface revisited:
₂ Stratified conditions and model-data comparisons**

Nicolas Rascle,^{1, 2} and Fabrice Ardhuin,¹

Nicolas Rascle, Centre Militaire d'Océanographie, Service Hydrographique et Océanographique
de la Marine, 29609 Brest, France

¹Centre Militaire d'Océanographie,
Service Hydrographique et Océanographique
de la Marine, 29609 Brest, France.

²Laboratoire de Physique des Océans,
Université de Bretagne Occidentale, 29000
Brest, France.

3 **Abstract.** A one-dimensional model of the ocean near-surface currents
4 is presented. It includes the enhanced near-surface mixing due to the waves,
5 the wave-induced Stokes drift, the Stokes-Coriolis effect and the stratifica-
6 tion. Near-surface current shears from this model are compared with the shears
7 of the quasi-Eulerian currents measured using a wave-following platform dur-
8 ing the Shelf Mixed Layer Experiment (SMILE). It is shown that the down-
9 wind current shears observed during SMILE are well modelled. However, the
10 observed crosswind shears are in poor agreement with the model. The Stokes-
11 Coriolis (SC) term could qualitatively explain this misfit but it is one order
12 of magnitude too weak. The Ekman-Stokes spiral of the model are compared
13 to the spiral observed during the long time series of measurements Long Term
14 Upper Ocean Study 3 (LOTUS 3). The effects of stratification are taken into
15 account. The mean velocity profiles of the model closely agree with obser-
16 vations. However, there is no evidence of the SC effect on the shape of the
17 observed Ekman spiral. The observed shape is found to be a consequence of
18 the rectification due to the stratification. The SC effect calculated from an
19 accurate numerical wave hindcast is weak, but should have been observed.
20 In fact, it is estimated that the wave-induced bias in the current measure-
21 ments is larger than the SC effect. Finally, it is shown that the variation of
22 surface drift with wave age, which was found to be small in unstratified con-
23 ditions, is important in the presence of shallow mixed layers.

1. Introduction

24 Breaking waves in the ocean can dramatically enhance near-surface mixing. This wave-
25 induced mixing was established from measurements of turbulent kinetic energy (TKE)
26 dissipation [*Agrawal et al.*, 1992; *Terray et al.*, 1996], and it was also observed in mea-
27 surements of downwind current vertical shear very close to the surface during the Shelf
28 Mixed Layer Experiment (SMILE) [*Santala*, 1991; *Terray et al.*, 2000]. As a result, the
29 surface mean current is rather weak, around 0.5% of the wind speed at 10 meters U_{10}
30 when the ocean is not stratified and when the waves are developed. This quasi-Eulerian
31 mean current is defined as the Lagrangian drift minus the wave Stokes drift [see *Jenkins*,
32 1987; *Rascle et al.*, 2006; *Ardhuin et al.*, 2008]. This small quasi-Eulerian drift can be
33 overwhelmed by large surface drift due to the wave Stokes drift [*Rascle et al.*, 2006, here-
34 inafter RAT06], which can be as large as 1.4% of U_{10} [see also *Rascle et al.*, 2008]. Other
35 processes likely contribute to the drift of surface-trapped buoyant objects that reaches
36 2 to 3% of U_{10} [*Huang*, 1979]. In the presence of stratification, the confinement of the
37 Ekman current near the surface may be an important factor.

38 Waves are also associated with a Stokes-Coriolis current [*Hasselmann*, 1970; *Xu and*
39 *Bowen*, 1994]. Namely, in a rotating frame of reference, a wave-induced stress perpendic-
40 ular to the waves propagation modifies the profile of the Ekman current. In an inviscid
41 ocean, this stress drives a mean current which compensates the Stokes drift of the waves
42 when averaged over the inertial period. However, in the presence of a strong vertical
43 mixing, this return flow is made vertically uniform. Because the Stokes drift of a wind sea
44 exhibits a strong vertical shear, the return flow only compensates the Stokes drift when

45 vertically integrated over depth, and there is a net drift at every depth. This was shown
46 in RAT06 without any stratification. Does this remain valid if the Ekman current is also
47 surface trapped, by a shallow mixed layer for instance?

48 The Stokes-Coriolis effect has never been clearly observed, except very close to the shore
49 from bottom-mounted ADCP's [*Lentz et al.*, 2008]. Evidence of this effect has been sought
50 by *Lewis and Belcher* [2004] and *Polton et al.* [2005] in the observations of the sub-surface
51 Ekman current during Long Term Upper Ocean Study 3 (LOTUS 3) [*Price et al.*, 1987].
52 Unfortunately, neither the wave-enhanced surface mixing nor the quite shallow diurnal
53 mixed layer during LOTUS 3 have been taken into account in their investigations, al-
54 though they can radically change the interpretation of the observed Ekman spiral [*Price*
55 *and Sundermeyer*, 1999]. Also, evidence of the Stokes-Coriolis forcing has not been sought
56 yet in measurements much closer to the surface, such as those of SMILE.

57
58 The present work builds on the modelling concepts proposed by RAT06. These include
59 a separation of near-surface flow into a wave Stokes drift and a quasi-Eulerian current. A
60 realistic vertical mixing is applied to the quasi-Eulerian current. This physical descrip-
61 tion leads to a different analysis of the near-surface current measurements whether they
62 are Lagrangian or Eulerian, because the Stokes drift was shown to be of same order as
63 the quasi-Eulerian current. RAT06 performed qualitative comparisons of modelled and
64 observed near-surface quasi-Eulerian currents and of sub-surface hodographs, showing en-
65 couraging results. However, those comparisons needed further analysis. For instance,
66 the near-surface quasi-Eulerian currents observed during SMILE were only compared to

67 model predictions in the downwind direction, and they took for granted the analysis of
 68 *Santala* [1991] (see section 3).

69 Here the effect of stratification is added to the model presented in RAT06, in order
 70 to make a quantitative comparison with the observations of near-surface current, and
 71 address the following questions: How well this model can reproduce the vertical shears
 72 observed close to the surface, both in the downwind and the crosswind direction? What is
 73 the impact of the Stokes-Coriolis effect on the Eulerian and Lagrangian current profiles in
 74 shallow mixed layers? Is there any observational evidence of this effect in the observations
 75 of Eulerian hodographs? What is the quantitative effect of shallow mixed layers on the
 76 surface drift?

77 The model used for this study is described in section 2. The near-surface shears of the
 78 quasi-Eulerian currents observed during SMILE are analyzed in section 3. The Ekman-
 79 Stokes spirals from the LOTUS 3 data are analyzed in section 4. Finally, the surface drift
 80 of the model in the presence of waves and stratification is discussed in section 5.

2. The model

The model used in the present study can be summarized as follows. Oceanic motions are separated in three components, mean flow, waves and turbulence. Turbulence is separated from other motions by a an average over flow realizations for given wave phases. The mean flow and wave motions are then averaged over the wave phases with a Generalized Lagrangian mean [*Andrews and McIntyre, 1978; Arduin et al., 2008*]. The horizontal total mean momentum \mathbf{U} is split in a quasi-Eulerian mean $\hat{\mathbf{u}}$ and a Stokes drift,

$$\mathbf{U} = \hat{\mathbf{u}} + \mathbf{U}_s. \quad (1)$$

81 Approximated to second order in the wave slope, the vertical profile of Stokes drift is
 82 given by the spectrum of the sea surface elevation, used here as a forcing for the model.
 83 Following *Ekman* [1905] we assume that the wave, velocity, and turbulent properties are
 84 uniform horizontally, which reduces the problem to the vertical dimension.

85 For the sake of simplicity and because we want to simulate a period of hundreds of
 86 days, a simple eddy viscosity model with a TKE closure scheme will be used. This model
 87 is adapted from *Craig and Banner* [1994, see also RAT06]. The wave-enhanced near-
 88 surface mixing is parameterized by the addition of a TKE flux at the surface, and the
 89 specification of a large sub-surface roughness length z_0 . The extension of this model to
 90 a stratified ocean is taken from *Noh* [1996] and following works [*Noh and Kim*, 1999;
 91 *Noh*, 2004]. The effects of stratification on the eddy diffusivities are parameterized via a
 92 turbulent Richardson number, where the conversion of TKE to potential energy is made
 93 regardless of the origin of turbulence, by shear production or by downward diffusion from
 94 the wave layer. This model was chosen for its ability to reproduce the diurnal thermocline.

The equations for the quasi-Eulerian horizontal momentum, for the mean buoyancy
 $B = -g\rho_w/\rho_0$ (g is the gravity acceleration, ρ_w the water density and ρ_0 a reference
 density) and for the mean turbulent kinetic energy E write [*Noh and Kim*, 1999]

$$\frac{\partial \hat{\mathbf{u}}}{\partial t} = -f\mathbf{e}_z \times (\hat{\mathbf{u}} + \mathbf{U}_s) + \frac{\partial}{\partial z} \left(K \frac{\partial \hat{\mathbf{u}}}{\partial z} \right), \quad (2)$$

$$\frac{\partial B}{\partial t} = \frac{\partial}{\partial z} \left(K_B \frac{\partial B}{\partial z} \right), \quad (3)$$

$$\frac{\partial E}{\partial t} = \frac{\partial}{\partial z} \left(K_E \frac{\partial E}{\partial z} \right) + K \left(\frac{\partial \hat{\mathbf{u}}}{\partial z} \right)^2 + K_B \left(\frac{\partial B}{\partial z} \right) - \frac{Cq^3}{l}, \quad (4)$$

where $q = \sqrt{2E}$ is the turbulent velocity scale, l is the mixing length, and where we
 used the eddy viscosity and diffusivity concepts. Those viscosity and diffusivities are

parameterized by

$$(K, K_B, K_E) = lq(S, S_B, S_E). \quad (5)$$

The proportionality constants (S, S_B, S_E, C) depend on the stratification via the introduction of a turbulent Richardson number [Noh, 2004]

$$Ri_t = \left(\frac{Nl}{q} \right)^2, \quad (6)$$

$$S = 0.39(1 + 5Ri_t)^{-1/2}, \quad (7)$$

$$S_B = S/0.8(1 + 0.5Ri_t)^{1/2}, \quad (8)$$

$$S_E = S/1.95, \quad (9)$$

$$C = 0.39^3(1 + 5Ri_t)^{1/2}, \quad (10)$$

95 where N is the Brunt-Väisälä frequency ($N^2 = -\partial B/\partial z$). Note that all proportionality
 96 constants (S, S_B, S_E, C) depend on the the turbulent Richardson number Ri_t and that
 97 the buoyancy diffusivity is multiplied by a Prandtl number which also depends on Ri_t .

The mixing length is parameterized as

$$l = \frac{\kappa(z_0 - z)}{1 + \kappa(z_0 - z)/h}, \quad (11)$$

98 where $\kappa = 0.4$ is the von Kármán's constant, h is the mixed layer depth, defined as the
 99 depth where the TKE is reduced by four orders of magnitude compared to its surface
 100 value [Noh, 2004], and z_0 is the roughness length. We use $z_0 = 1.6H_s$ as in Terray *et al.*
 101 [2000]. H_s is the significant wave height of the wind sea, a proxy for the scale of the
 102 breaking waves that are responsible for the mixing.

The boundary conditions at the mean sea level ($z = 0$) are

$$K \frac{\partial \hat{\mathbf{u}}}{\partial z} \Big|_{z=0} = u_*^2, \quad (12)$$

$$K_B \frac{\partial B}{\partial z} \Big|_{z=0} = Q \quad (13)$$

$$K_E \frac{\partial E}{\partial z} \Big|_{z=0} = \Phi_{oc}, \quad (14)$$

103 where u_* is the waterside friction velocity, Q is the surface downward buoyancy flux and
 104 Φ_{oc} is the surface downward TKE flux. Following to *Terray et al.* [1996], the TKE flux is
 105 parameterized as $\Phi_{oc} = \alpha u_*^3$, with $\alpha = 100$.

106 The bottom has almost no effect on the near surface dynamics, provided that the depth
 107 is substantially greater than both Stokes and Ekman depths and than the mixed layer
 108 depth. Therefore, the bottom boundary layer is not described here.

109 Those equations are solved with a time step of $dt = 10$ s and a vertical discretization of
 110 $dz = 1$ m. Each variable are collocated, the space differentials are expressed in standard
 111 second order centrally differenced forms and the time step is implicit.

112 Justification for the use of such a simple eddy viscosity model can be found by comparing
 113 the velocity profiles of the model to the velocity profiles of more sophisticated models like
 114 the large eddy simulations (LES) of *McWilliams et al.* [1997] or *Noh et al.* [2004]. Such
 115 comparisons have shown reasonable agreement [e.g. *Kantha and Clayson*, 2004].

3. Analysis of the near-surface shears - The SMILE data

3.1. The experiment

116 The SMILE experiment was described in details by *Santala* [1991] and only a short
 117 review will be given here. The experiment took place on the Northern California shelf in
 118 1988-1989. It included measurements of oceanographic and atmospheric variables using
 119 moored platforms. One measurement of particular interest was made with the Surface
 120 Acoustic Shear Sensor (SASS), a wave-following device which included velocity measure-

121 ments very close to the surface, at depths smaller than H_s . In our analysis, we will focus
122 on those SASS measurements, ignoring the longer and deeper measurements from conven-
123 tional moorings made during the same field experiment and we will use the abbreviation
124 SMILE to refer to the SASS measurements only. The SASS buoy is a rigid array designed
125 specifically to follow the surface elevation. It was moored over the shelf in 90 m depth,
126 at the location ($38^{\circ}39'$ N, $123^{\circ}29'$ W). Currents relative to the buoy were measured at
127 depths 1.11, 2.51, 3.11 and 5.85 m using 4 acoustic current meters. Gyroscopes and ac-
128 celerometers were used to determine the motion of the buoy relative to the inertial frame
129 of reference. The resulting measurements of currents referred to the inertial frame are
130 unique with respect to their proximity of the surface. The currents were averaged over
131 40 mn. Horizontal average velocities were corrected for a wave-induced bias due to correla-
132 tions between the SASS motion and the wave orbital velocities, estimated from measured
133 wave spectra (see also section 4.6 for a physical description of the wave-induced bias).
134 The velocities were also corrected for estimated errors due to flow distortions induced by
135 the structure.

136 Here we focus on 13 records averaged over 40 mn, spread during the afternoon and
137 night on February 27, 1989. The average wind speed was $U_{10} = 13.6 \text{ m s}^{-1}$ and the
138 average wave height was $H_s = 2.3 \text{ m}$, both approximately aligned (from the North West,
139 300°) and steady. The wave peak period was $T_p = 7.8 \text{ s}$, which corresponds to a wave
140 age $C_p/U_{10} = 0.89$, where C_p is the wave phase speed at the spectral peak. The com-
141 bined measurements of temperature with the SASS and with the nearby conventional
142 mooring show that water column was unstratified down to 20 m depth. To parameterize
143 the atmospheric boundary layer, *Santala* [1991] used local observations and extrapolated

144 missing observations, such as the air temperature, from distant buoy measurements. He
 145 calculated the stability parameter $-\kappa Z/L$ [*Large and Pond, 1981*], where $Z = 7$ m is
 146 the elevation above the sea surface and $L = u_*^3/Q$ the Monin-Obukhov length scale, and
 147 obtained values comprised between 0 and -0.03 . The corresponding downward surface
 148 heat flux Q_h is thus between 0 and -8 W m $^{-2}$. Using a similar combination of in-situ
 149 measurements and bulk formulae, *Beardsley et al. [1998]* found that the shortwave heat
 150 flux roughly compensated the longwave, latent and sensible heat loss, giving a small daily
 151 mean surface heat flux on February 27-28, around $+30$ W m $^{-2}$ (given the uncertainty of
 152 visual reading of *Beardsley et al. [1998]*'s fig. 6). We will thus neglect this small heat flux,
 153 given the large values of the Monin-Obukhov length scale (93 m).

3.2. The model

154 The model is run with the steady observed mean wind speed. The temperature is
 155 initialized with the observed stratification, with a thermocline around 20 m, and a zero
 156 surface heat flux is used. The Stokes-Coriolis force is estimated by assuming that the sea
 157 state conforms to a JONSWAP spectrum [*Hasselmann et al., 1973; Kudryavtsev et al.,*
 158 *1999*], with a fetch of 100 km which gives the observed H_s . The peak period of waves is
 159 slightly underestimated with this method, giving $T_p = 6.4$ s whereas 7.8 s was observed.
 160 The Stokes transport of the waves, important to measure the magnitude of the Stokes-
 161 Coriolis force, might then be overestimated. The model results, averaged over one inertial
 162 period, are shown in fig. 1 (upper panel). For comparison, the model results without
 163 stratification are plotted on fig. 1 (lower panel).

3.3. Previous analysis of the SMILE data

164 The measurements have already been analyzed by *Santala* [1991], and part of its results
165 were used by *Terray et al.* [2000] and RAT06. Here we will briefly summarize their analysis
166 and the different method used here.

167 Four velocity sensors were mounted on the SASS buoy, at depths from 1 to 5 m. The
168 vertical shear can be estimated with the finite difference of velocities between pairs of
169 adjacent sensors. *Santala* [1991] scaled the depth with u_*^2/g . This is equivalent to a
170 significant wave height H_s scale, provided that swells are excluded in H_s and assuming
171 that the wind sea is fully developed. The shear was scaled with u_*/z , the "law of the
172 wall" scaling. These scalings yield their fig. 7-5, which we reproduce here for the SASS
173 data only (fig. 2).

174 The analysis of this plot, together with deeper measurements from a conventional moor-
175 ing, leads these authors to infer a description of the downwind shear in a 3 layer structure,
176 namely an upper layer with almost no shear, a lower layer following a log-law and a tran-
177 sition layer in between. However, such a transition is hardly perceptible with only the
178 SASS data, because the lowest shear estimate falls in the transition region (fig. 2, upper
179 panel). In the crosswind direction, the shear was found roughly constant with depth. This
180 analysis leads to the figure 7-11 in *Santala* [1991], which was reproduced in *Terray et al.*
181 [2000] and RAT06, showing the current profiles inferred from this analysis. These profiles
182 were used afterwards in the discussion of *Santala* [1991].

3.4. New analysis of the SMILE data

183 It is not obvious from fig. 2 that the fit to the finite-difference estimated shears produces
184 a reliable value of the mean shear. Due to the wave-induced mixing, the near-surface

185 vertical shear should better be scaled with u_*/H_s [*Craig and Banner, 1994*]. Even with
186 this scaling, vertical profiles of the current shear remain quite noisy (fig. 3).

187 A more robust estimation of the mean vertical shear is given by a linear regression to
188 the current measured at all 4 sensors. The choice of a linear profile corresponds to the
189 constant near-surface shear expected in the wave-mixed layer [*Craig and Banner, 1994*,
190 equ. 30]. By imposing the vertical structure of the shear, this estimation method avoids
191 the spreading due to finite difference shear estimations. It also reduces drastically the
192 scatter between the 13 records, as shown in fig. 4.

193 The observed and modelled shears are shown in fig. 5, with the elevation scaled by H_s
194 and the current by u_* . In the downwind direction (fig 5, upper panel) the observed shear,
195 scaled by u_*/H_s , is 0.42 ± 0.26 , where the first number is the mean and the second is
196 the standard deviation. The corresponding downwind shear of the model is 0.23 with the
197 full model. If the wave-enhanced near-surface mixing is omitted in the model (by using a
198 small roughness length $z_0 = 5$ cm and by setting the TKE surface flux to zero), the shear
199 reaches 1.52. As was noted in *Terray et al. [2000]* and RAT06, those observations of quite
200 weak near-surface downwind shears are consistent with an intense wave-induced mixing.

201 In the crosswind direction (fig. 5, lower panel) the mean non-dimensional observed
202 shear is -0.52 ± 0.31 . The corresponding crosswind shear of the full model is -0.030 ,
203 which is one order of magnitude smaller than the observations.

204 The Stokes-Coriolis force, oriented in the crosswind direction, is a possible explanation
205 for that large observed crosswind shear, because it is oriented to the right of the waves
206 propagation, as is the observed shear bias. Therefore we made a quantitative evaluation of
207 the Stokes-Coriolis impact on the crosswind current. The wave field is not fully developed.

208 The Stokes transport is around 10% of the Ekman transport, which means, according to
209 *Polton et al.* [2005], that the Stokes-Coriolis effect is equivalent to a surface stress of
210 10% of the wind stress. The consequent crosswind shear (fig 5, lower panel) is quite
211 small, increasing from -0.014 without the Stokes-Coriolis force to -0.030 with it. An
212 upper bound of the Stokes-Coriolis stress can be found by supposing the wave field fully
213 developed. The equivalent stress is then 35% of the wind stress, but the crosswind shear
214 only reaches -0.041 (fig. 5, lower panel). The Stokes-Coriolis force is thus too weak
215 to explain the large crosswind observed shears, and this is a consequence of the strong
216 wave-induced mixing imposed in the model. Namely, if we omit the wave-induced mixing
217 in the model, the crosswind shear reaches -0.21 without the Stokes-Coriolis force, -0.31
218 with it and even -0.37 when supposing maximum value of the Stokes-Coriolis force, in
219 better agreement with the observed shear. The SMILE observations of crosswind shear
220 thus appear inconsistent with the wave-induced enhancement of the mixing, contrary to
221 the downwind shear observations.

222 Explanation for this asymmetry of crosswind and downwind shear observations might
223 be found in anisotropic momentum transfert from wave breaking or in anisotropic wave-
224 induced turbulence, in the presence of Langmuir circulations especially. The velocity
225 profiles of different LES simulations of Langmuir turbulence (*McWilliams et al.* [1997],
226 *Noh et al.* [2004],...) suggest that the mixing due to Langmuir cells is not isotropic. This
227 is beyond the scope of the present numerical simulation.

228 Also, if Langmuir circulations were present, the SASS buoy could have been trapped
229 into surface convergence zones. *Santala* [1991] investigated the vertical velocity records
230 and did find a non-zero mean downward velocity, interpreted as evidence of a non-uniform

231 sampling of the Langmuir cells. The consequent bias on the horizontal velocity measure-
232 ment cannot be excluded to explain the large observed crosswind shear.

4. Analysis of the current magnitude - The LOTUS data

233 The impact of the Stokes-Coriolis effect and of the stratification is small on the current
234 shear, but is more apparent on the magnitude of the current : the Ekman transport is
235 trapped in the mixed layer, leading to large values of the crosswind current, while the
236 Stokes-Coriolis effect gives small values, if not negative, of the downwind current (see e.g.
237 fig. 1, upper panel). Are the observed current in agreement with that expected shape?

238 Field measurements of the Ekman currents are always noisy, due to inertial oscillations
239 and various other phenomena, some of them being surface-trapped. It is thus difficult to
240 separate other processes from the mean wind-driven current. During SMILE (previous
241 section), the currents were averaged over 40 mn. This allows an analysis of the vertical
242 shears but it is insufficient to investigate the magnitude of the current. One solution to
243 get rid of this noise is to average the current over a long time period. This method has
244 been employed by *Price et al.* [1987] with the LOTUS 3 data set.

245 The LOTUS 3 experiment took place in the western Sargasso Sea (34° N, 70° W) in the
246 summer of 1982, under light to moderate winds, $U_{10} = 5.4 \pm 2.7 \text{ m s}^{-1}$, and strong diurnal
247 heating, with an average of the daily maximum net surface heat flux of 630 W m^{-2} [*Price*
248 *and Sundermeyer, 1999*]. The current measurements came from Vector Measuring Current
249 Meters (VMCMs) along a conventional mooring, with the upper measurements at 5, 10,
250 15 and 25 m depth. In the typical light wind encountered, waves were small, $H_s =$
251 $1.3 \pm 0.7 \text{ m}$, so that the wave-induced bias, i.e. the correlation between the motion of
252 the mooring and the orbital motion of the waves, was first estimated to be small at

253 the measurement depths using VMCMs [*Schudlich and Price, 1998*]. We will further
254 discuss this point below. Finally *Price et al. [1987]* used a coherent averaging method to
255 follow the low frequency changes in wind direction. The resulting current profile can then
256 be quantitatively compared to theoretical models of the Ekman current. This observed
257 current has the expected profile of an Ekman spiral, with a depth integrated transport in
258 agreement with the Ekman transport. However, some features were unexpected. First,
259 the sub-surface deflection is quite large, around 75° at a depth of 5 m. Second, the decay
260 with depth is stronger than the clockwise rotation (the spiral is 'flat').

261 To explain this flatness of the spiral, *Price and Sundermeyer [1999]* invoked the temporal
262 variation of stratification. The mixed layer depth varied typically from 10 m during the
263 day to 25 m at night. The mean current, time-averaged over the diurnal cycle, is thus
264 rectified, and exhibits a different vertical profile than the current inferred from the mean
265 vertical stratification [see also *McWilliams and Huckle, 2006*].

266 Later, *Lewis and Belcher [2004]* and *Polton et al. [2005]* noted that the approach of *Price*
267 *and Sundermeyer [1999]* is not able to reconcile the observed large sub-surface deflection
268 of 75° and a small surface deflection of 10 to 45° typically observed from drifting objects
269 [*Huang, 1979*]. Ignoring the stratification, *Lewis and Belcher [2004]* and *Polton et al.*
270 *[2005]* argued that the Stokes-Coriolis force can explain the large sub-surface deflection,
271 together with a small surface deflection. The agreement between their models and the
272 LOTUS 3 observations was then quite good [see *Polton et al., 2005*, their fig. 8].

273 Other problems appear in turn in these models. First, the small surface deflections
274 reviewed in *Huang [1979]* mainly come from observations of Lagrangian surface drift. As
275 noted in RAT06, the Lagrangian surface drift is the sum of the Stokes drift and the quasi-

276 Eulerian current. A large surface deflection of the quasi-Eulerian current is not contrary to
 277 a small surface deflection of the Lagrangian drift, because of the Stokes drift. In relation
 278 to this, the surface mixing in the models of *Lewis and Belcher* [2004] and *Polton et al.*
 279 [2005] is likely to be several orders of magnitude too small. But, as noted in RAT06
 280 without stratification, a realistic surface mixing gives a quasi-Eulerian current much more
 281 uniform than modelled by the previous authors, ruining the agreement with the data (see
 282 RAT06, fig. 7). Stratification is therefore needed to reexamine the LOTUS 3 data. Here
 283 we also reexamine whether or not the LOTUS 3 data offer an observational evidence of
 284 the Stokes-Coriolis effect on the Ekman current.

4.1. A simple model of the diurnal cycle

285 Following the idealized model of *Price and Sundermeyer* [1999], the present model is
 286 run with the mean wind stress observed during the period, $u_* = 0.0083 \text{ m s}^{-1}$. The waves
 287 are expected to be fully developed with that wind stress, which gives a significant wave
 288 height of $H_s = 1.6 \text{ m}$, based on the spectrum of *Kudryavtsev et al.* [1999].

The temperature is initialized with the temperature observed at the beginning of the field experiment. For the surface heat flux, we use an analytical fit of the solar insolation measured during clear sky days and we suppose that a steady heat loss equilibrates the surface heat budget,

$$Q = \max \left(0, 1000 \cos \left(\frac{2\pi t}{T_{day}} \right) \right) - \frac{1000}{\pi}, \quad (15)$$

289 where t is the time and T_{day} is a period of one day.

290 The mixed layer depth h is calculated using the model criteria $E(h) < E(z = 0) \times 10^{-4}$.
 291 The probability density function (PDF) of the mixed layer depth is shown in fig. 6,

292 showing a bimodal distribution corresponding to diurnal and nocturnal mixed layers.
293 With these mean wind stress, surface heat flux and initial temperature, the mixed layer
294 depth varies between 8 m and 40 m, as observed during LOTUS 3 (fig. 6). However
295 the vertical profile of the current is very different from the observed one. The modelled
296 current is too large and homogeneous within the mixed layer (fig. 7).

297 Not surprisingly, the velocity profile is not well reproduced when we use the mean wind
298 stress. The rectification over sub-periods with weak wind should not leave a mean velocity
299 profile homogeneous in the upper 8 m. Similarly, if a strong wind event occurred during
300 the measurement period, its effect must be apparent on the mean velocity profile below
301 30 m deep.

4.2. A more elaborate model: using the wind history

302 The previous results using the average wind stress are encouraging but the profile of
303 the mean current exhibits a large sensitivity to the mixed layer depth history. The tem-
304 perature variability is not well reproduced with only a simple reproduction of the diurnal
305 cycle. We will therefore attempt a more realistic simulation of the LOTUS 3 data, using
306 the full recorded history of the wind stress.

307 For computational simplicity, the wind direction is taken constant, in agreement with
308 the coherent averaging of *Price et al.* [1987]. This simplification can be further justified
309 by the absence of any clear indication of what the damping of inertial oscillations should
310 be in a one dimensional model [e.g. *Mellor*, 2001]. The bulk formulation of COAMPS
311 [*Hodur et al.*, 2002] for the atmospheric boundary layer is used to calculate the wind
312 stress. The relative humidity is set to 75%, as in *Stramma et al.* [1986]. The wind stress
313 is 6 hours low-pass filtered. Using the filtered wind stress and not the filtered wind speed

314 conserves the stress and minimizes the rectification errors. Finally, the current of the
315 model, averaged over one hour, is stored and used to calculate the mean over the whole
316 time period (170 days).

317 When one wants to reproduce the stratification, both the heat budget and the large
318 scale advection of heat come into play. Attempting to validate their 1D model of the
319 ocean vertical mixing, *Gaspar et al.* [1990] analyzed a 2 weeks subset of the LOTUS 3
320 measurements. They reported imbalance of the order of 80W m^{-2} in the ocean heat bud-
321 get. They estimated large scale advection to be responsible for an imbalance of 15W m^{-2} .
322 Remaining errors were attributed to the bulk derived heat fluxes and uncertain estima-
323 tions of latent heat flux [see *Stramma et al.*, 1986] and of solar infrared flux, due to missing
324 measurements of relative humidity and of cloud type, respectively.

325 These uncertainties on the advection and heat flux are critical for a simulation of the
326 observed temperature, as the model temperature might slowly drift away from observa-
327 tions. However, the present study investigates currents, for which the mixed layer depth
328 is more important than the absolute value of the temperature. The analytical heat flux
329 (15) and the observed wind stress may suffice to produce an adequate mixed layer history.
330 During day time the model yields good results (fig. 6), as the thickness of the diurnal
331 mixed layer is determined by the Monin-Obukhov length scale, i.e. by the surface heat
332 and momentum fluxes. However, the nocturnal convection and its effect on stratification
333 are also determined by the temperature profile and the water column heat content, espe-
334 cially when the nocturnal heat loss exceeds the preceding diurnal heat gain. The small
335 drift of the model temperature, when attempting a long time simulation of the LOTUS 3

336 experiment with the analytical heat flux (15), leads to large over-estimations of nocturnal
337 mixed layer depth predictions (fig. 6).

4.3. A pragmatic model: Constraining the stratification

338 In order to avoid errors due to differences in stratification, we will constrain the tem-
339 perature to the observed temperature. Every 6 hours, we re-initialize the temperature
340 of the model to the 1-hour mean observed temperature. The analytical fit (15) for the
341 heat flux is still used to reproduce the high-frequency diurnal cycle. The temperature of
342 the simulation is therefore in close agreement with the observed temperature (correlation
343 coefficient above 0.99 at every measurement depth), including the diurnal stratification,
344 except during a few episodes of exceptionally weak solar insolation not captured with our
345 simple heat flux (15).

4.4. Model results

346 The comparison between the modelled current averaged over the entire period and the
347 coherent averaging of observations by *Price and Sundermeyer* [1999] is very good (fig. 7
348 and 8). The crosswind current agrees well with the observations, with differences less than
349 0.36 cm s^{-1} ($= 0.45u_*$) and relative errors of less than 10% for the 3 upper measurements.
350 The crosswind transport of the model is equal to the Ekman transport, corresponding
351 to the mean wind stress, while the crosswind transport calculated with a trapezoidal
352 extension of the data is slightly (8%) inferior [see also *Price et al.*, 1987]. The downwind
353 current of the model, if we omit the Stokes-Coriolis effect, is in correct agreement with
354 the observations, with differences less than 0.47 cm s^{-1} ($= 0.58u_*$) which still represent
355 relative errors of the order of 100%. The downwind transport of the model without the

356 Stokes-Coriolis effect is nil, and the downwind transport from the extrapolated data is
357 around $-1.9 \times 10^{-3} \text{ m}^2 \text{ s}^{-1}$, which is 0.26% of the crosswind Ekman transport.

358 Such agreement between the model and the observations is encouraging. It provides
359 the opportunity to estimate the importance of the different ingredients of the model. In
360 particular, we test the model sensitivity to the roughness length. As shown in fig. 7,
361 the mean velocity profile is mainly determined by the stratification and the consequent
362 rectification effect. The wave-induced mixing is less discernable on velocity measurements
363 below 5 m depth than above, and at those depth it is hard to discriminate between small
364 and large values of the roughness length.

4.5. The Stokes-Coriolis effect

365 The Stokes drift has been calculated by supposing the wave field fully developed with
366 the corresponding wind averaged over 6 hours. This gives an upper bound of the Stokes-
367 Coriolis effect (fig. 8, dotted line).

368 A more realistic estimation of that effect is also needed. The complete historic of the
369 waves during the period is preferable, because it includes possible correlations between
370 large wave events, strong wind events and particular stratification events like deep mixed
371 layers. Therefore, a global wave model of 1° resolution is used to produce the sea state at
372 the LOTUS 3 station (34.0N, 70.0W). The wave model is based on the WAVEWATCH
373 III (WW3) code [Tolman *et al.*, 2002], in which the wind-wave evolution parameteriza-
374 tions have been replaced by those of Bidlot *et al.* [2005]. Although these parameteriza-
375 tions still have some problems in costal and swell-dominated areas [Ardhuin *et al.*, 2007],
376 they provide good results for the mean parameters H_s and T_{m02} when compared to the
377 North Atlantic buoys measurements [Ardhuin and Le Boyer, 2006; Rascle *et al.*, 2008;

378 *Bidlot et al.*, 2007]. This model is forced with 10-m winds 6-hourly ERA 40 re-analysis
379 [*Uppala et al.*, 2005] from the European Center for Medium-Range Weather Forecasting
380 (ECMWF). The comparison with the nearby buoy 41001 (34.7N, 72.7W) of the National
381 Data Buoy Center (NDBC) shows an rms error of 0.43 m on H_s (25% of the rms H_s) and
382 of 0.57 s on the mean period T_{m02} (9.8% of the rms T_{m02}), for the period from 14 May
383 to 30 November 1982. Note that no wave data were available at that buoy from 6 June
384 to 6 August. Our calculation might underestimate the Stokes transport since there is a
385 significant negative bias on the wave height H_s (-0.25 m), and a negligible bias on the
386 mean period T_{m02} (-0.07 s).

387 The wave spectra at the LOTUS 3 station were used to compute the Stokes drift.
388 Consistently with the average of *Price et al.* [1987] which follows the wind direction, we
389 need to rotate the Stokes drift components according to the wind rotation. To avoid any
390 discrepancy between the observed wind direction and the reanalyzed wind direction, we
391 need to use the ERA 40 wind direction. Because at the surface the Stokes drift is a high
392 moment of the spectrum, it is almost aligned with the wind. For computational simplicity,
393 this surface Stokes drift direction is taken as a proxy for the ERA 40 wind direction.
394 Furthermore, the average of the Stokes drift (rotated following the wind rotation) over
395 the whole time period is found to be aligned with the wind, with a mean crosswind Stokes
396 transport of 2.3% of the downwind Stokes transport. It means that the mean contribution
397 of waves not aligned with the wind, swell for instance, is weak. For additional simplicity,
398 we thus use the norm of the Stokes drift and prescribe it aligned with the wind at each
399 depth at every time step. This second simplification leads to an increase of the mean

400 downwind Stokes transport by 2.6%, which is negligible compared to the uncertainties of
401 the waves reanalysis.

402 The numerical results with that estimation of the Stokes-Coriolis term are shown in
403 fig. 8. The mean Stokes transport is $0.075 \text{ m}^2 \text{ s}^{-1}$, i.e. 9.5% of the Ekman transport
404 which reaches $0.79 \text{ m}^2 \text{ s}^{-1}$. Accordingly, the mean downwind current transport of the
405 model with the Stokes-Coriolis effect is $-0.91 \text{ m}^2 \text{ s}^{-1}$, which compensates the Stokes
406 transport (within a 17% error which may be due to insufficient vertical discretization or
407 rectification). On the contrary the downwind transport from the extrapolated data is
408 almost nil ($-1.9 \times 10^{-3} \text{ m}^2 \text{ s}^{-1}$).

409 Similarly, the downwind current profile of the model is closer to the data when we omit
410 the Stokes-Coriolis term (fig. 8). In this regard, the present work is consistent with the
411 work of *Price and Sundermeyer* [1999], showing that the 'flatness' of the spiral results
412 from the stratification, in contradiction to *Polton et al.* [2005], who claimed that it is due
413 to the Stokes-Coriolis effect.

4.6. The wave-induced bias

One explanation emerges for that apparent misfit of the model when including the Stokes-Coriolis effect: the observed downwave velocities were supposed to be Eulerian but could have been contaminated by the wave-induced buoy motion. Namely, the mooring line measured 5395 m in 5366 m of water and was thus very taut. One can then consider that the sub-surface currentmeter motion follows the surface buoy motion, and this should yield a wave-induced bias due to correlations between orbital wave motion and currentmeter motion. *Schudlich and Price* [1998] used the method of *Santala* [1991] to discuss that wave-induced bias. In particular, one can suppose that the buoy moves

vertically with the surface. Then, for each monochromatic wave train, one gets in addition to the quasi-Eulerian current a bias equal to

$$\Delta u_{min}(z) = \frac{1}{2}a^2\omega k \exp(-kz), \quad (16)$$

where z is the elevation measured downward, a is the wave amplitude, ω is the radian frequency and k the wavenumber. This gives a lower bound of the wave-induced bias. Assuming that the buoy moves both vertically and horizontally, the maximum wave-induced bias is

$$\Delta u_{max}(z) = a^2\omega k \exp(-kz). \quad (17)$$

For comparison, the Stokes drift of a monochromatic wave is

$$U_s(z) = a^2\omega k \exp(-2kz). \quad (18)$$

414 As the wave-induced motions of the current meters are larger than the wave-induced
 415 motions of the particles, the maximum bias is larger than the Stokes drift (the equality
 416 arises at the surface only, see fig. 9, left panel).

417 The wave spectrum predicted by the wave model gives the average over the whole
 418 LOTUS 3 period of Δu_{min} and Δu_{max} (fig. 9, left panel). Those biases have also been
 419 added to the downwind current of the model with the Stokes-Coriolis effect (fig. 9, right
 420 panel, thin lines).

The vertical integral of the bias is bounded by

$$M^w \leq \int_{-H}^0 \Delta u dz \leq 2M^w, \quad (19)$$

421 where M^w is the Stokes transport ($= a^2\omega/2$ for a monochromatic wave). Therefore, as
 422 the theoretical downwind transport is equal to $-M^w$, the biased transport is comprised

423 between 0 and $+M^w$ (fig. 9, right panel, thin lines). The observed downwind transport in
424 LOTUS 3 is approximately zero. It was interpreted by *Price et al.* [1987] as an evidence
425 that the Ekman transport is crosswind. But the transport induced by the Stokes-Coriolis
426 effect is not negligible (9.5% of the Ekman transport) and should have been observed.
427 We argue here that it was not observed because of the wave-induced bias. Furthermore,
428 in the winter measurements of LOTUS 4, a positive downwind transport was found and
429 was interpreted by *Schudlich and Price* [1998] as a wave-induced bias, coming from the
430 large winter waves. The present description supports the more nuanced conclusion that
431 both the LOTUS 3 and the LOTUS 4 measurements are likely biased by the waves in the
432 downwind direction.

5. Surface drift

433 One aim of the present model is a better understanding of the surface Lagrangian
434 drift, for applications to search and rescue, fish larvae recruitment or any other studies
435 following floating materials. The present model, following *Garrett* [1976] and *Jenkins*
436 [1989], separates the flow into a wave Stokes drift and an Eulerian current. In particular,
437 the introduction of the wave age should bring new insight in the near-surface dynamics.
438 One remarkable result obtained in RAT06 for unstratified conditions is that the surface
439 drift is almost independent of the wave age : as the waves gets more mature, the Stokes
440 drift increases. But the mixing is also more efficient and leaves an Ekman current more
441 homogeneous, thus reducing the surface quasi-Eulerian current and compensating the
442 increase of the Stokes drift. This result is recalled in fig. 10 (upper panel, for $Q_h = 0$;
443 note that the quasi-Eulerian current is weaker at the surface compared to results obtained

444 in fig. 12 in RAT06 due to the poorer vertical resolution, the first level being at -0.5 m
445 in the present model).

446 Whereas the wave age is a key parameter for the near-surface mixing, it has little
447 influence on the surface drift in unstratified conditions. A simple parameterization of
448 the surface drift directly from the wind might then be possible. But this result does not
449 hold in stratified conditions. The dependance of the surface drift on the wave age in the
450 presence of strong stabilizing buoyancy flux ($Q_h = 1000 \text{ W m}^{-2}$, which gives a Monin-
451 Obukhov length scale $L = 0.24$ m) is shown in fig. 10. For strong buoyancy forcing, the
452 mixed layer is shallow (around $8 - 12$ m) so that the quasi-Eulerian surface current is
453 almost crosswind (angle around -90°). Consequently, the reduction of the quasi-Eulerian
454 current, when waves get more developed and mixing more efficient, is not compensated
455 by the increase of the Stokes drift of the waves, contrary to what happens in unstratified
456 conditions where the angle between the Stokes drift and the quasi-Eulerian current is
457 more modest (angle around 45°). In addition, the mixed layer of the model gets thicker
458 with a larger wave-induced mixing (from 8 m for short fetches to 12 m for large fetches),
459 which further increases the wave age dependance of the surface drift during strong heating
460 events. The surface drift thus reaches 3% of the wind speed U_{10} for very shallow mixed
461 layer associate with small fetches. That mixed layer depth dependency on the wave age is
462 physically sound but requires further verifications. Useful validation data were acquired
463 during the C-BLAST experiment off the U.S. East Coast and are still being processed
464 (T.P. Stanton, Naval Postgraduate School, Monterey, CA, personal communication).

6. Conclusion

465 A model of the surface layer of the ocean was presented in RAT06. Essentially, the
466 current was separated into a wave Stokes drift and a quasi-Eulerian current. That physical
467 description led to a different analysis of the observations of currents profiles close to
468 the surface, whether the measurements are Eulerian or Lagrangian. That analysis agreed
469 qualitatively with a few available data of Lagrangian drift profiles, of Eulerian velocity
470 profiles and of TKE dissipation rates. Motivated by these results, this work is extended
471 here by including the stratification, allowing a more quantitative validation of the current
472 profiles.

473 We performed a reanalysis of the near-surface quasi-Eulerian velocity measurements
474 during SMILE. The near-surface shears were previously investigated under the hypothesis
475 of a 3 layer structure [*Santala*, 1991]. Here we made no hypothesis on the structure of
476 the shear and we linearly interpolate the upper current measurements. The near-surface
477 shears obtained are found to be in good agreement with the downwind shears expected
478 in the presence of a strong wave-induced mixing. However, crosswind shears found are
479 an order of magnitude larger than expected. These large crosswind shears cannot be
480 explained by the Stokes-Coriolis force, which is one order of magnitude too weak. Models
481 and complementary observations of Langmuir cells appear therefore to be necessary for
482 further investigations of these near-surface current measurements.

483 The long term observations of Ekman spirals during LOTUS 3 provide an opportunity to
484 investigate the Stokes-Coriolis effect. The use of a long time series reduces the noise in the
485 measurement, enabling an analysis of the magnitude of the wind-driven current. However,
486 it introduces rectification effects because of the temporal variations of the wind and of the
487 stratification. The wind variability is taken into account by using the coherent averaging

488 of *Price et al.* [1987], which follows the wind direction, and changes in the stratification are
489 represented by constraining the temperature to the observed temperature. The Ekman
490 spiral of the model then shows very good agreement with the observations. However, we
491 do not find any evidence of the Stokes-Coriolis effect, whereas accurate wave hindcasts
492 suggest that it should be significant, leading to upwind transport around 10% of the
493 crosswind Ekman transport. The nature of the measurement is then in question, because
494 the bias induced by the waves on near-surface measurements from a buoy can be larger
495 than the Stokes transport. Seeking evidence of the Stokes-Coriolis effect such long time
496 averaging, as attempted by *Lewis and Belcher* [2004] and *Polton et al.* [2005], still appears
497 to be feasible but preference should be accorded to measurements from fixed towers to
498 get rid of that wave-induced bias.

499 Finally, we investigated the surface drift predictions of the model in the presence of
500 stratification. It is shown that the wave age effect on the surface drift, which was found to
501 be small in unstratified conditions, is important in the presence of shallow diurnal mixed
502 layers. In such case, considering separately the wave field and the mean current should
503 give significant differences on surface drift predictions.

504 **Acknowledgments.** The initial version of the computer code for the mixed layer model
505 was kindly provided by Yign Noh. We acknowledge the National Buoy Data Center
506 (NDBC) and the Upper Ocean Mooring Data Archive of the Woods Hole Oceanographic
507 Institution (WHOI) for their web-available data. N.R. acknowledges the support of a
508 CNRS-DGA doctoral research grant.

References

- 509 Agrawal, Y. C., E. A. Terray, M. A. Donelan, P. A. Hwang, A. J. Williams, W. Drennan,
510 K. Kahma, and S. Kitaigorodskii (1992), Enhanced dissipation of kinetic energy beneath
511 breaking waves, *Nature*, *359*, 219–220.
- 512 Andrews, D. G., and M. E. McIntyre (1978), An exact theory of nonlinear waves on a
513 Lagrangian-mean flow, *J. Fluid Mech.*, *89*, 609–646.
- 514 Ardhuin, F., and A. Le Boyer (2006), Numerical modelling of sea states: validation of
515 spectral shapes (in French), *Navigation*, *54*(216), 55–71.
- 516 Ardhuin, F., T. H. C. Herbers, K. P. Watts, G. P. van Vledder, R. Jensen, and H. Graber
517 (2007), Swell and slanting fetch effects on wind wave growth, *J. Phys. Oceanogr.*, *37*(4),
518 908–931, doi:10.1175/JPO3039.1.
- 519 Ardhuin, F., N. Rascle, and K. A. Belibassakis (2008), Explicit wave-averaged primi-
520 tive equations using a generalized lagrangian mean, *Ocean Modelling*, *20*, 35–60, doi:
521 10.1016/j.ocemod.2007.07.001.
- 522 Beardsley, R. C., E. P. Dever, S. J. Lentz, and J. P. Dean (1998), Surface heat flux
523 variability over the northern california shelf, *J. Geophys. Res.*, *103*, 21 553 –21 586.
- 524 Bidlot, J., S. Abdalla, and P. Janssen (2005), A revised formulation for ocean wave dis-
525 sipation in CY25R1, *Tech. Rep. Memorandum R60.9/JB/0516*, Research Department,
526 ECMWF, Reading, U. K.
- 527 Bidlot, J.-R., et al. (2007), Inter-comparison of operational wave forecasting systems, in
528 *Proceedings, 10th Int. Workshop of Wave Hindcasting and Forecasting, Hawaii*.
- 529 Craig, P. D., and M. L. Banner (1994), Modeling wave-enhanced turbulence in the ocean
530 surface layer, *J. Phys. Oceanogr.*, *24*, 2546–2559.

- 531 Ekman, V. W. (1905), On the influence of the earth's rotation on ocean currents, *Ark.*
532 *Mat. Astron. Fys.*, *2*, 1–53.
- 533 Garrett, C. (1976), Generation of Langmuir circulations by surface waves - a feedback
534 mechanism, *J. Mar. Res.*, *34*, 117–130.
- 535 Gaspar, J. P., Y. Grégoris, and J. M. Lefevre (1990), A simple eddy kinetic energy model
536 for simulations of oceanic vertical mixing : Tests at station papa and long-term upper
537 ocean study site., *J. Geophys. Res.*, *95*(C9), 16,179–16,193.
- 538 Hasselmann, K. (1970), Wave-driven inertial oscillations, *Geophys. Fluid Dyn.*, *1*, 463–502.
- 539 Hasselmann, K., et al. (1973), Measurements of wind-wave growth and swell decay during
540 the Joint North Sea Wave Project, *Deut. Hydrogr. Z.*, *8*(12), 1–95, suppl. A.
- 541 Hodur, R. M., J. Pullen, J. Cummings, X. Hong, J. D. Douyle, P. J. Martin, and M. A.
542 Rennick (2002), The coupled ocean/atmosphere mesoscale prediction system (coamps),
543 *Oceanography*, *15*, 88–98.
- 544 Huang, N. E. (1979), On surface drift currents in the ocean, *J. Fluid Mech.*, *91*, 191–208.
- 545 Jenkins, A. D. (1987), Wind and wave induced currents in a rotating sea with depth-
546 varying eddy viscosity, *J. Phys. Oceanogr.*, *17*, 938–951.
- 547 Jenkins, A. D. (1989), The use of a wave prediction model for driving a near-surface
548 current model, *Deut. Hydrogr. Z.*, *42*, 133–149.
- 549 Kantha, L. H., and C. A. Clayson (2004), On the effect of surface gravity waves on mixing
550 in the oceanic mixed layer, *Ocean Modelling*, *6*, 101–124.
- 551 Kudryavtsev, V. N., V. K. Makin, and B. Chapron (1999), Coupled sea surface-
552 atmosphere model. 2. spectrum of short wind waves, *J. Geophys. Res.*, *104*, 7625–7639.

- 553 Large, W. G., and S. Pond (1981), Open ocean momentum flux measurements in moderate
554 to strong winds, *J. Phys. Oceanogr.*, *11*, 324–336.
- 555 Lentz, S. J., M. Fewings, P. Howd, J. Fredericks, and K. Hathaway (2008), Observations
556 and a model of undertow over the inner continental shelf, *J. Phys. Oceanogr.*, pp. ???–
557 ???
- 558 Lewis, D. M., and S. E. Belcher (2004), Time-dependent, coupled, Ekman boundary layer
559 solutions incorporating Stokes drift, *Dyn. Atmos. Oceans*, *37*, 313–351.
- 560 McWilliams, J. C., and E. Huckle (2006), Ekman layer rectification, *J. Phys. Oceanogr.*,
561 *36*, 1646–1659.
- 562 McWilliams, J. C., P. P. Sullivan, and C.-H. Moeng (1997), Langmuir turbulence in the
563 ocean, *J. Fluid Mech.*, *334*, 1–30.
- 564 Mellor, G. L. (2001), One-dimensional, ocean surface layer modelling: A problem and a
565 solution, *J. Phys. Oceanogr.*, *31*, 790–809.
- 566 Noh, Y. (1996), Dynamics of diurnal thermocline formation in the oceanic mixed layer,
567 *J. Geophys. Res.*, *26*, 2189–2195.
- 568 Noh, Y. (2004), Sensitivity to wave breaking and the Prandtl number in the ocean
569 mixed layer model and its dependence on latitude, *Geophys. Res. Lett.*, *31*, L23,305,
570 doi:10.1029/2004GL021289.
- 571 Noh, Y., and H. J. Kim (1999), Simulations of temperature and turbulence structure of
572 the oceanic boundary layer with the improved near-surface process, *J. Geophys. Res.*,
573 *104*(C7), 15,621–15,634.
- 574 Noh, Y., H. S. Min, and S. Raasch (2004), Large eddy simulation of the ocean mixed
575 layer: the effects of wave breaking and Langmuir circulation, *J. Phys. Oceanogr.*, *34*,

- 576 720–733.
- 577 Polton, J. A., D. M. Lewis, and S. E. Belcher (2005), The role of wave-induced Coriolis-
578 Stokes forcing on the wind-driven mixed layer, *J. Phys. Oceanogr.*, *35*, 444–457.
- 579 Price, J. F., and M. A. Sundermeyer (1999), Stratified Ekman layers, *J. Geophys. Res.*,
580 *104*(C9), 20,467–20,494.
- 581 Price, J. F., R. A. Weller, and R. R. Schudlich (1987), Wind-driven ocean currents and
582 Ekman transport, *Science*, *238*, 1534–1538.
- 583 Rascle, N., F. Ardhuin, and E. A. Terray (2006), Drift and mixing under the ocean surface.
584 a coherent one-dimensional description with application to unstratified conditions, *J.*
585 *Geophys. Res.*, *111*, C03,016, doi:10.1029/2005JC003004.
- 586 Rascle, N., F. Ardhuin, P. Queffelec, and D. Croiz-Fillon (2008), A global wave parame-
587 ter database for wave-current-turbulence interaction studies, *Ocean Modelling*, submit-
588 ted.
- 589 Santala, M. J. (1991), Surface referenced current meter measurements, Ph.D. thesis,
590 Woods Hole Oceanographic Institution and the Massachusetts Institute of Technology,
591 WHOI-91-35.
- 592 Schudlich, R. R., and J. F. Price (1998), Observations of seasonal variation in the Ekman
593 layer, *J. Phys. Oceanogr.*, *28*, 1187–1204.
- 594 Stramma, L., P. Cornillon, R. A. Weller, J. F. Price, and M. G. Briscoe (1986), Large
595 diurnal sea surface temperature variability : Satellite and in situ measurements, *J.*
596 *Phys. Oceanogr.*, *16*, 827–837.
- 597 Terray, E. A., M. A. Donelan, Y. C. Agrawal, W. M. Drennan, K. K. Kahma, A. J.
598 Williams, P. A. Hwang, and S. A. Kitaigorodskii (1996), Estimates of kinetic energy

- 599 dissipation under breaking waves, *J. Phys. Oceanogr.*, *26*, 792–807.
- 600 Terray, E. A., W. M. Drennan, and M. A. Donelan (2000), The vertical structure of
601 shear and dissipation in the ocean surface layer, in *Proc. Symp. on Air-Sea Interaction,*
602 *Sydney*, pp. 239–245, University of New South Wales.
- 603 Tolman, H. L., B. Balasubramaniyan, L. D. Burroughs, D. V. Chalikov, Y. Y. Chao, H. S.
604 Chen, and V. M. Gerald (2002), Development and implementation of wind-generated
605 ocean surface wave models at NCEP, *Weather and Forecasting*, *17*(4), 311–333.
- 606 Uppala, S. M., et al. (2005), The ERA-40 re-analysis, *Quarterly Journal of the Royal*
607 *Meteorological Society*, *131*, 2961–3012, doi:10.1256/qj.04.176.
- 608 Xu, Z., and A. J. Bowen (1994), Wave- and wind-driven flow in water of finite depth, *J.*
609 *Phys. Oceanogr.*, *24*, 1850–1866.

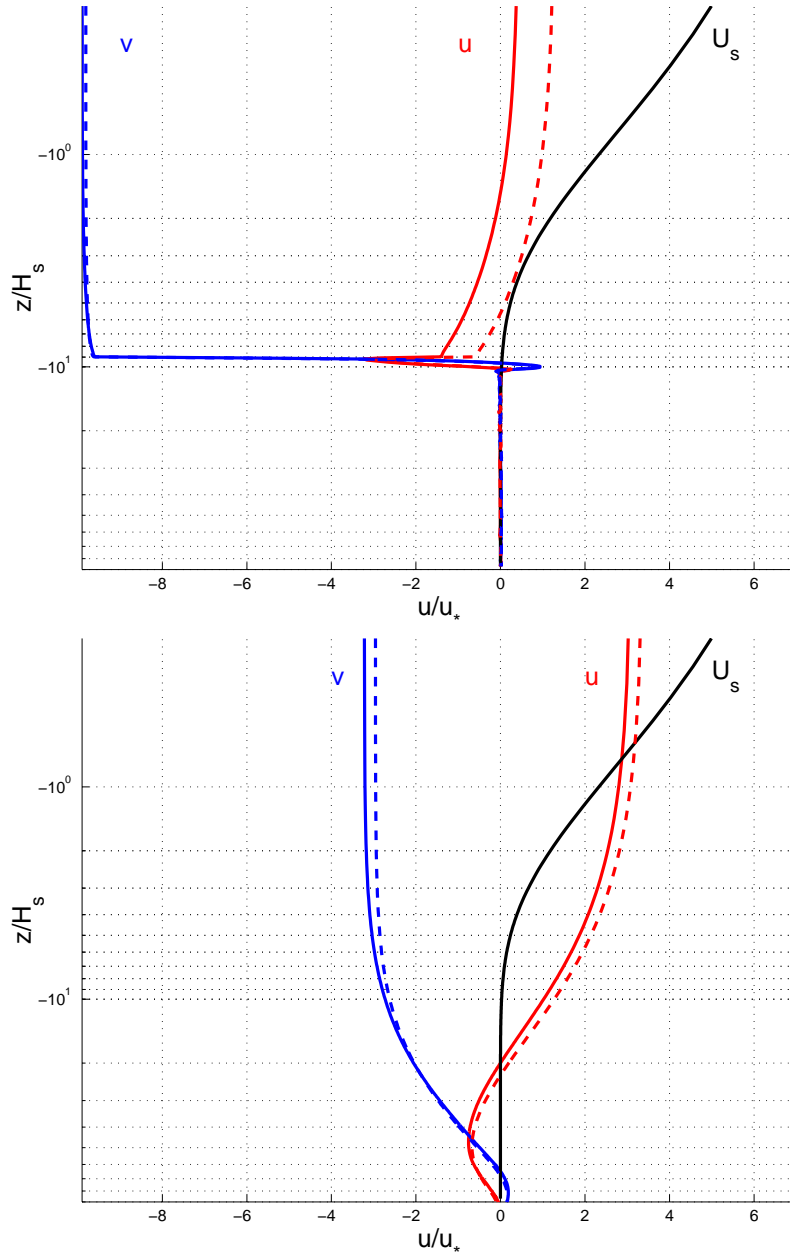


Figure 1. Velocity profiles from the model. \hat{u} is the downwind quasi-Eulerian velocity, \hat{v} is the crosswind quasi-Eulerian velocity and U_s is the Stokes drift. Velocities and elevation are normalized by the waterside friction velocity u_* and by the significant wave height H_s , respectively. Solid lines and dashed lines are model results with and without the Stokes-Coriolis effect, respectively. Upper panel is with a 20 m deep mixed layer as observed during SMILE and lower panel is without the effect of stratification.

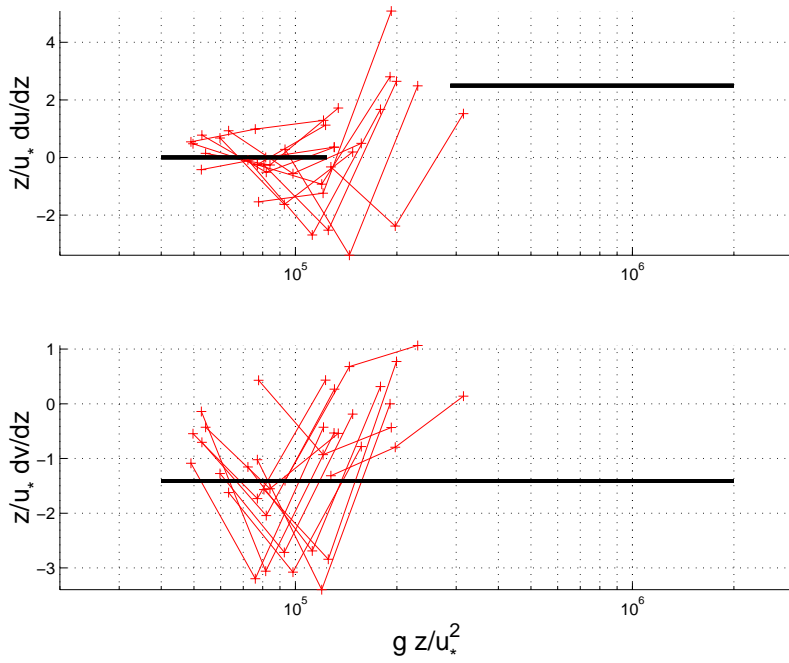


Figure 2. Reproduction of the Figure 7-5 of *Santala* [1991], for the SASS data only. Nondimensional variation of shear with depth for the downwind (upper panel) and for the crosswind (lower panel) directions. The + and thin lines are measurements from the SASS, the thick solid lines are the shears inferred in the original analysis of *Santala* [1991], with the 3 layers structure in the downwind direction.

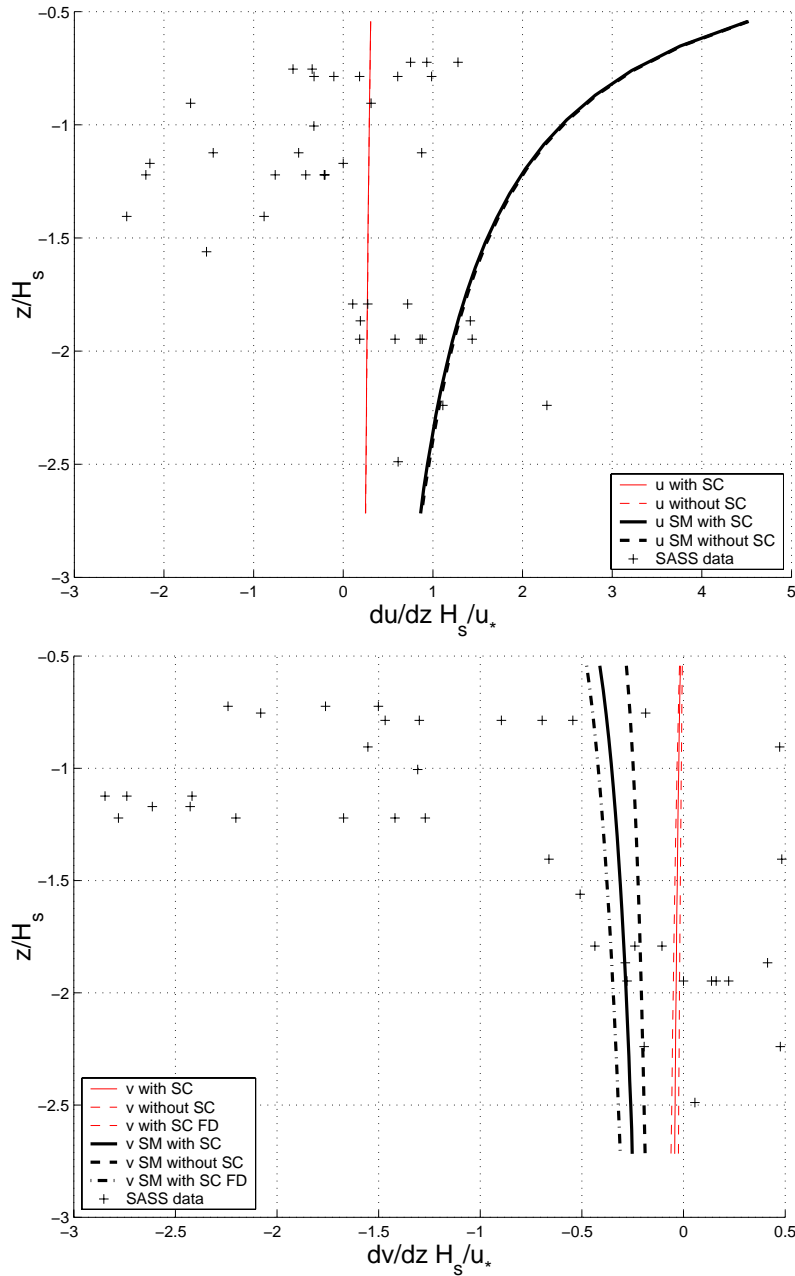


Figure 3. (Upper panel) Shear of the downwind component u of the current, normalized with u_*/H_s , plotted as function of the depth normalized with H_s . Shears of the model are calculated by finite difference and shears of the SASS data are calculated by finite difference between each pairs of adjacent sensors. In addition to the default model results, we plotted the results of the model without the Stokes-Coriolis effect (SC) or/and without the wave-induced surface mixing (SM= Small Mixing), obtained with a roughness length of $z_0 = 0.05$ m and no TKE surface flux. (Lower panel) Same as upper panel but for the crosswind component v of the current. As an upper bound of the Stokes-Coriolis effect, the model results when supposing the wave field fully developed (FD) is also shown.

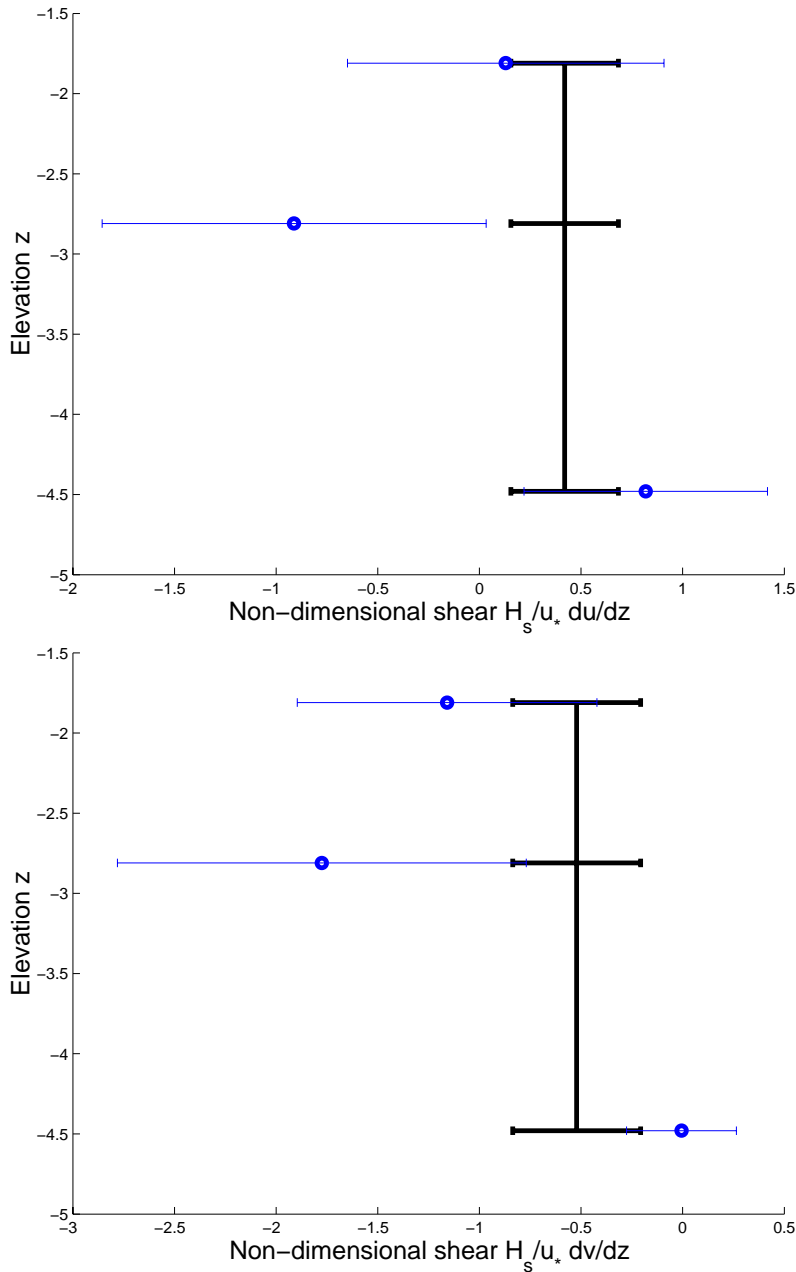


Figure 4. (Upper panel) Shear of the downwind component u of the current, normalized with u_*/H_s , plotted as function of the depth. Dots are shears calculated by finite difference between each pairs of adjacent sensors. Thick line is shear obtained from linear interpolation of the current velocities over the 4 current-meter depths. We show mean values over the set of 13 records with error bars representing standard deviations. (Lower panel) Same as upper panel but for the crosswind component v of the current.

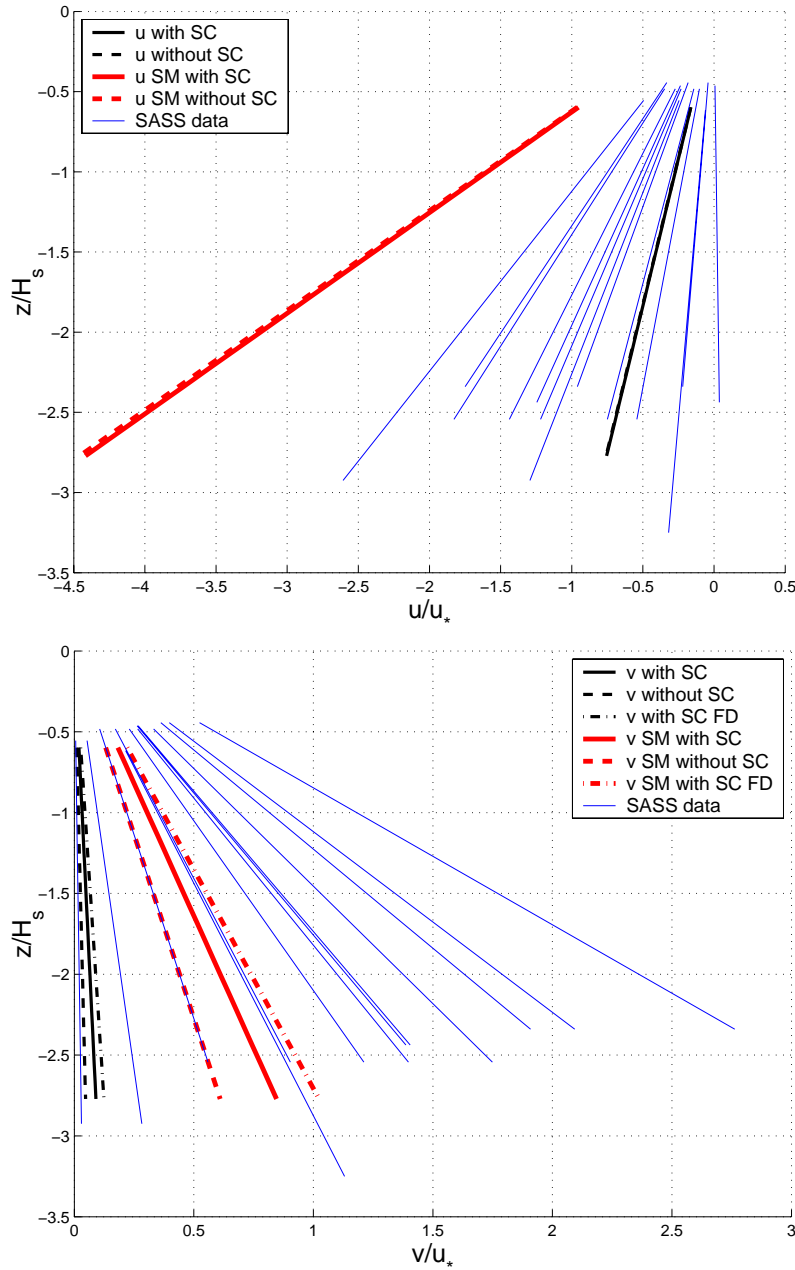


Figure 5. (Upper panel) Linear regression of the downwind current u between 1.1 m and 5.8 m deep, the measurement depths of the SASS buoy. The current is normalized with u_* and the depth with H_s . The SASS data are plotted, as well as different model results. In addition to the default model results, we plotted the results of the model without the Stokes-Coriolis effect (SC) or/and without the wave-induced surface mixing (SM= Small Mixing), obtained with a roughness length of $z_0 = 0.05$ m and no TKE surface flux. (Lower panel) Same as upper panel but for the crosswind component v . The SASS data are plotted, as well as different model results. (As in fig 3, lower panel, SC is Stokes-Coriolis, SM is Small Mixing and FD is Fully Developed waves.)

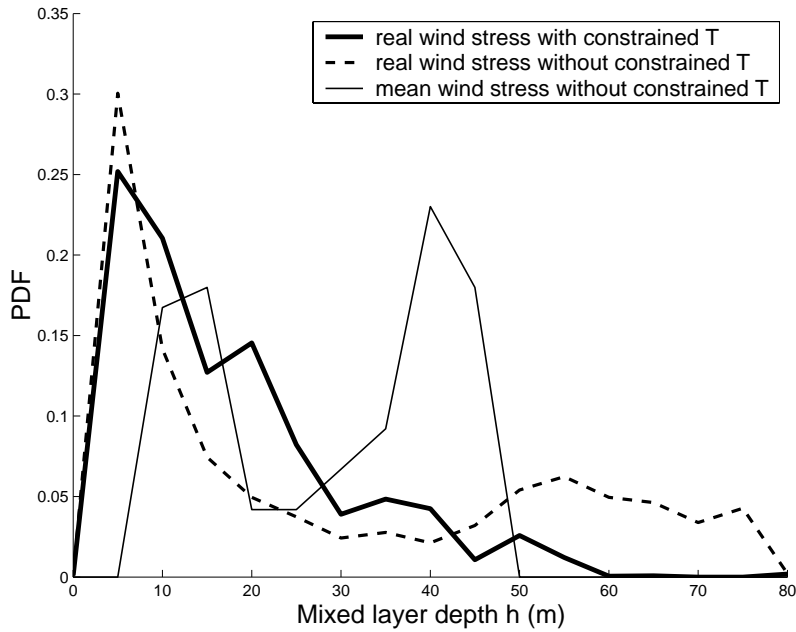


Figure 6. Probability density functions of the hourly mixed layer depth of 3 numerical simulations of the LOTUS 3 measurement. The mixed layer depth is defined with a criteria on attenuation of surface TKE [Noh, 2004]. All model runs use the analytical heat flux (15), which closes the heat budget. Thin solid line is the model with the mean observed wind stress (section 4.1), dashed line is with the observed variable wind (section 4.2), thick solid line is with the observed wind and with the temperature assimilation (section 4.3).

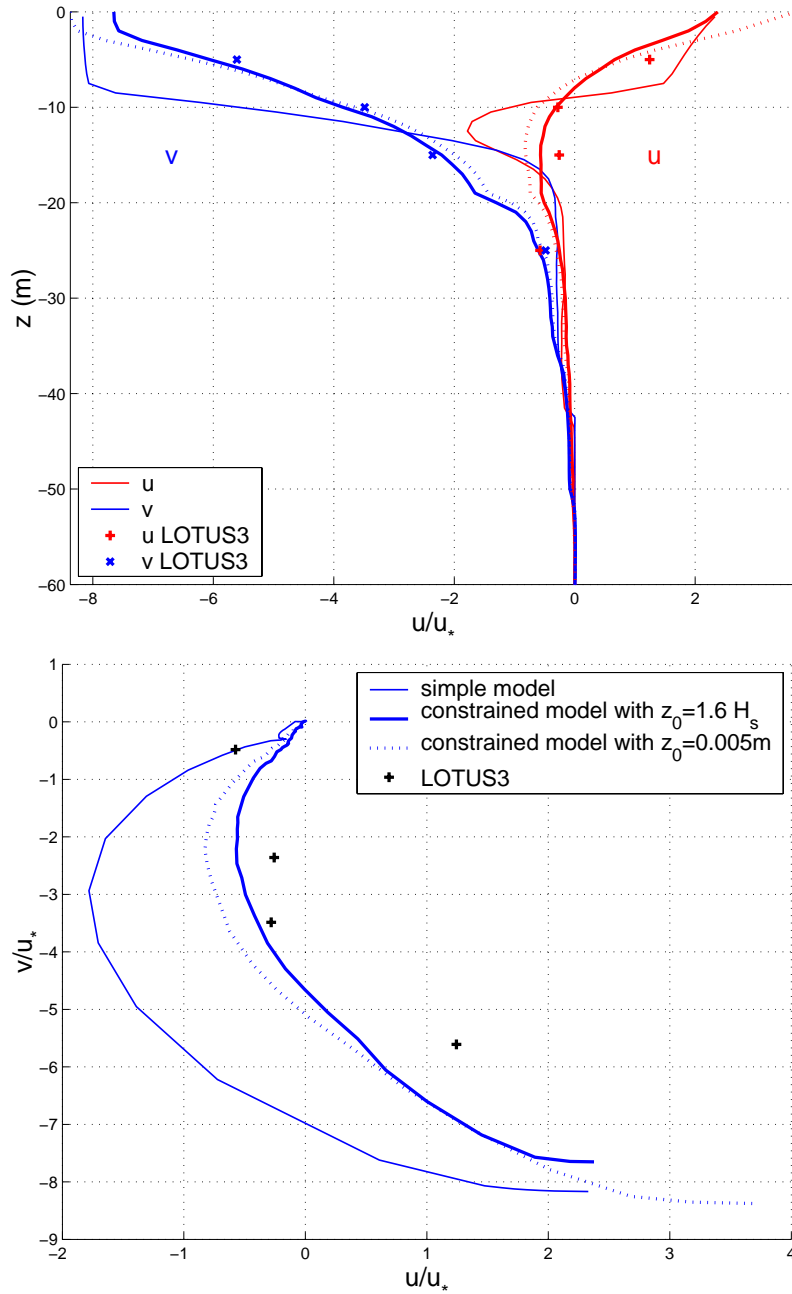


Figure 7. Mean currents obtained in three different LOTUS 3 simulations, each without the Stokes-Coriolis force. Upper panel shows vertical profiles of the mean current (\hat{u} , \hat{v}). Lower panel shows hodographs of the mean current. Each simulation uses the analytical heat flux (15). Thin line uses the mean wind stress (section 4.1). Thick solid and dotted lines use the variable wind stress and the constrained temperature (section 4.3), and test the sensitivity to the the wave-induced mixing with roughness lengths $z_0 = 1.6H_s$ and $z_0 = 0.005$ m, respectively.

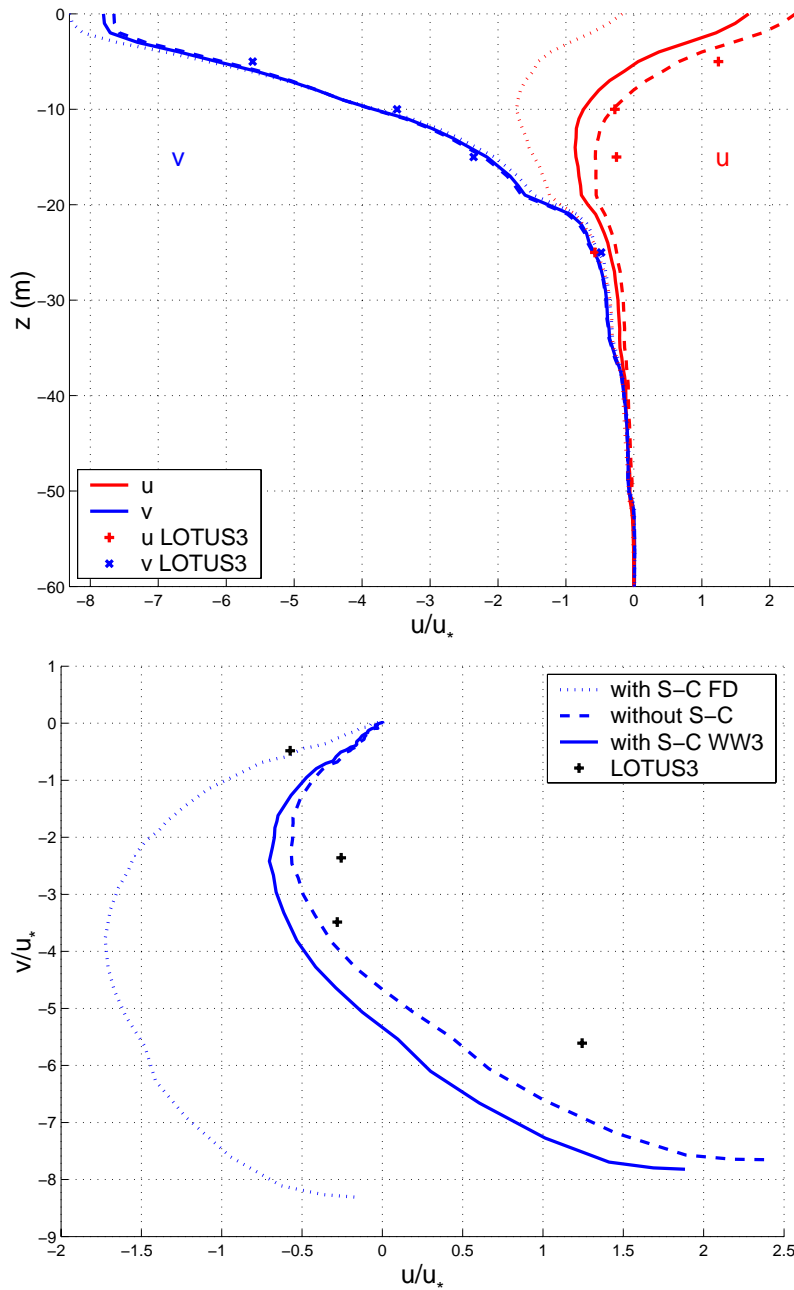


Figure 8. LOTUS 3 simulation, using the observed wind stress and with the temperature constrained to the data. Upper panel shows vertical profiles of the mean current (\hat{u} , \hat{v}). Lower panel shows hodographs of the mean current. Dashed lines are the model results without the Stokes-Coriolis effect. Dotted lines are the model results when supposing the waves fully developed (with the 6 hours low-pass filtered wind), giving an upper bound of the Stokes-Coriolis effect. Solid lines represent model results with the Stokes-Coriolis effect calculated using the WW3 wave hindcast.

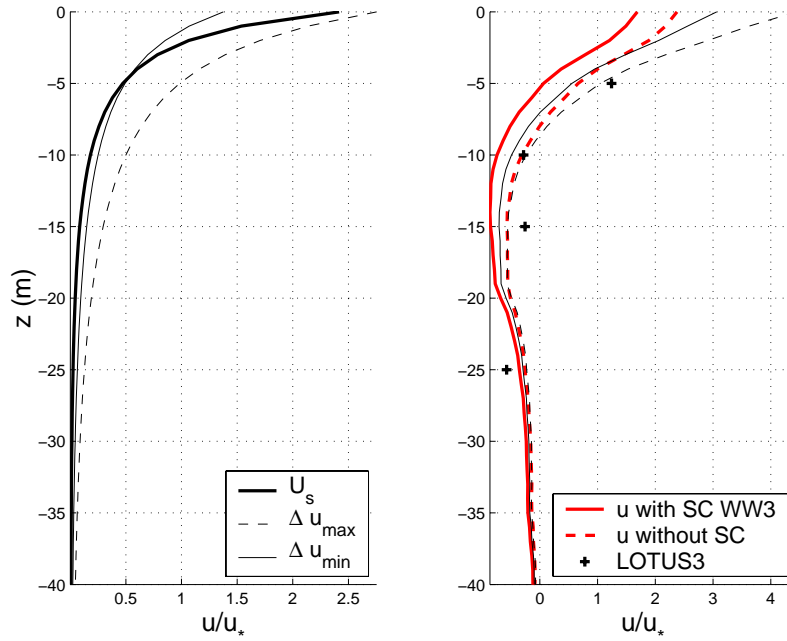


Figure 9. Wave-induced bias on the LOTUS 3 measurements. (Left panel) Vertical profiles of the averaged norm of the Stokes drift U_s (thick solid line), of Δu_{max} (thin dashed line) and of Δu_{min} (thin solid line). (Lower panel) Profile of velocity \hat{u} calculated with the Stokes-Coriolis effect from the wave reanalysis (thick solid line, similar to fig. 8), augmented with the additional bias Δu_{min} (thin solid line) and Δu_{max} (thin dashed line). Also shown is the velocity \hat{u} calculated without the Stokes-Coriolis effect (thick dashed line, similar to fig. 8).

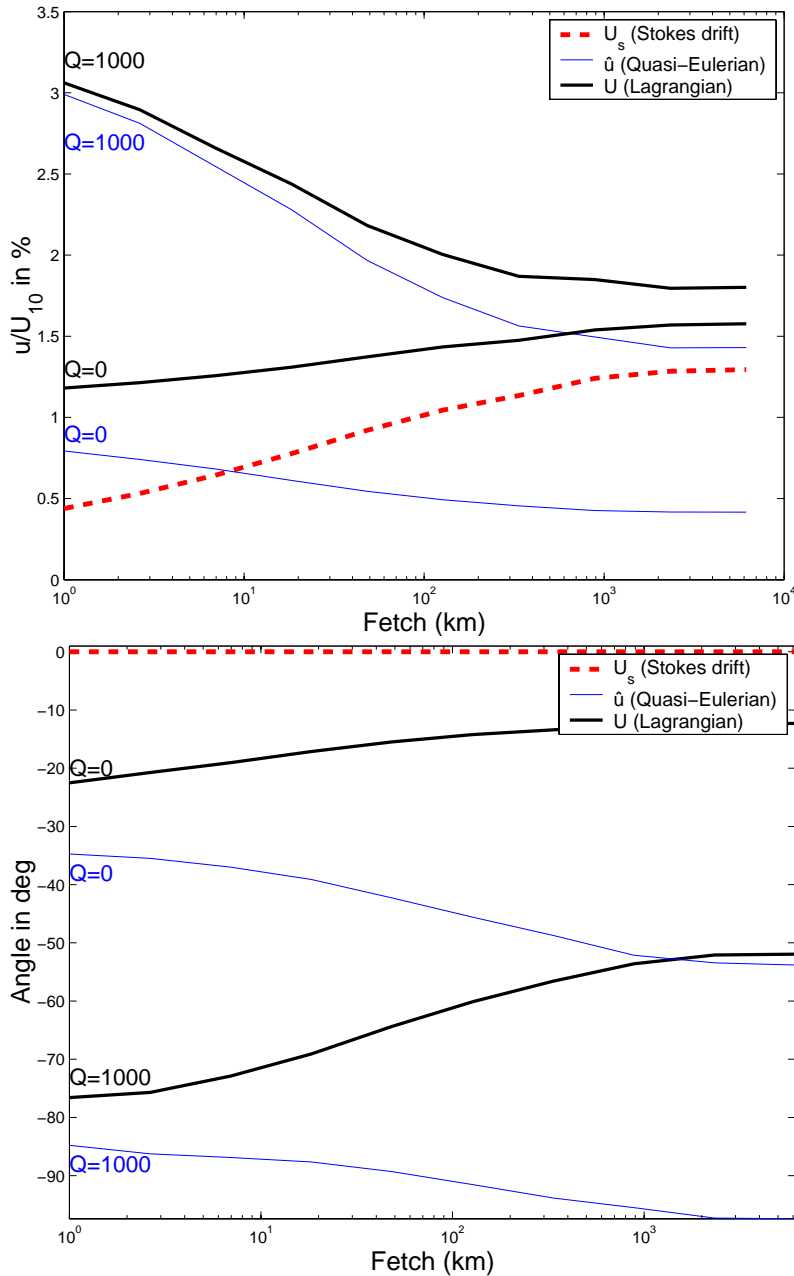


Figure 10. (Upper panel) Stokes drift \mathbf{U}_s , quasi-Eulerian current $|\hat{\mathbf{u}}|$ and total Lagrangian drift $\mathbf{U} = |\hat{\mathbf{u}} + \mathbf{U}_s|$ at the surface ($z = -0.5$ m), as function of fetch. The velocities are expressed as a percentage of the wind speed U_{10} . The wind is set to $U_{10} = 10\text{ms}^{-1}$, and two different stratifications are obtained from an initially uniform density and applying two different surface heat fluxes, $Q_h = 0$ and $Q_h = 1000 \text{ W m}^{-2}$. (Lower panel) Corresponding angles of deviations from the wind direction, measured counterclockwise.